

The Collective Physics of Motile Cells in Complex Environments

Ross Edwards

Level 4 Project, MSci Natural Sciences

Supervisor: Professor S. Fielding

Second Supervisor: Dr. M. Hertaeg

Department of Physics, Durham University

Abstract

Biological tissue shows mechanical properties intermediate between solid and liquid: when probed on short timescales, it shows elastic solid-like response. On longer timescales, it reshapes itself and ‘flows’. It is also unlike conventional materials in that its constituent particles (biological cells) are autonomously active, in being able to crawl, grow and divide. This results in fascinating phenomena in the collective physics of biological cells, during (e.g.) embryo development, wound healing and tumour invasion. This computational project explores the collective physics of active cells by employing an agent-based active matter model of their behaviour. In particular, we study the role of collective, stochastic cell behaviour in the emergence of periodic tissue fingering from a circular monolayer bound by a Lennard-Jones potential. Although inconclusive, we find that, from a bidisperse system, there is a narrow range of magnitude of random activity that generates localised periodic fingers. However, we find no evidence of reproducible periodic tissue fingering from a monodisperse system.



Contents

1	Introduction	3
1.1	Active Matter Systems	3
1.2	Research Objectives	4
2	Self-Organization in Motile Cell Systems	5
2.1	Cell Clustering Behaviour	5
2.2	Biological Tissue Fingering	7
3	Research Models for Motile Cell Behaviour	9
3.1	Stochastic Motion	9
3.2	Pairwise Soft Harmonic Repulsion	12
3.3	Lennard-Jones Interactions	16
4	Results & Discussion	20
4.1	Cell Activity Affects Cluster Stability	20
4.2	Periodic Protrusions Occur at a Critical Activity	22
4.3	Bidispersity	25
4.4	Tissue Growth	26
5	Conclusion & Future Perspectives	27
References		28
Acknowledgements		31

1 Introduction

The study of motile cells in complex environments, driven by computational modelling, is a growing area of research that encompasses multiple subfields within the broader discipline of biophysics. Cells collectively display self-organizing patterns and emergent phenomena [1] that, when studied, help to elucidate the underlying mechanisms driving biological systems of interest. This thesis aims to clearly present and discuss the results of research into the emergence of periodic tissue fingering from a population of motile cells represented by a biological, agent-based active matter model. Tissue fingering simply describes the development of finger-like protrusions from a main body of cells, and is a phenomenon that occurs as cells become active and collectively migrate [2]. By investigating the origin of tissue fingers, we can better understand how tissues migrate and coordinate motion, which is crucial for a range of vital biological processes, including wound healing, tumour invasion, and embryonic development [3, 4, 5]. Therefore, establishing a comprehensive understanding of the core mechanisms that govern tissue fingering may aid the advancement of therapeutic development for these processes.

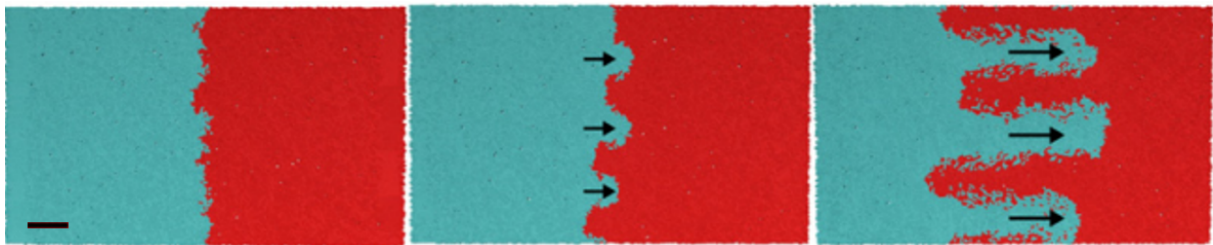


Figure 1: Example snapshots of interface undulations, resembling finger-like protrusions, that arise as one tissue migrates into another for increasing motility force strength (left to right) [2]. The scale bar represents 10 cell diameters.

1.1 Active Matter Systems

Active matter systems, such as flocks of birds, active colloids, and biological tissue, comprise a large set of self-propelled entities that interact with each other and their environment, and convert stored energy into mechanical work to transition the system away from thermal equilibrium

[6]. Although they are all characterized as non-equilibrium systems, active matter differs from field-driven or sheared systems in that, in these examples, the mechanical work of individual constituents is instead derived from external forces [7, 8]. To model active matter, researchers use tools from statistical mechanics, soft matter physics, and hydrodynamics. Statistical mechanics is used to describe the behaviour of systems with a large number of interacting particles [9], while soft matter physics enables the study of materials with properties that do not solely belong to either solids or liquids [10]. Finally, the use of mathematical equations derived from the field of hydrodynamics is essential for building more complex systems that involve motion within a fluid, or fluid-like, medium [6].

The collective behaviour of active matter emerges from the interactions and feedback mechanisms between their individual constituents. This can give rise to non-equilibrium phase transitions, which are novel phenomena characterised by the emergence of new macroscopic properties and patterns [11]. In the context of biological research, non-equilibrium phase transitions can occur during tissue migration as cells exchange mechanical energy with their neighbours and their surroundings. This is seen in the emergence of tissue fingering, which is the subject of our research. In summary, active matter models are able to capture large-scale physics and emergent collective behaviour from a population of self-propelling agents that are each treated as individual entities. This is highly applicable to our research as we choose to represent our cells as individual elements, rather than adopting an active fluid model that treats groups of cells as a continuous fluid [12].

1.2 Research Objectives

The main objective of this research is to assess the fundamental origin of periodic tissue fingering from clusters of motile cells. Specifically, we aim to investigate the extent to which distinct tissue fingering patterns may arise purely as a result of random activity in the collective behaviour of motile cells, as, historically, this phenomenon has been attributed to the presence of ‘leader cells’ (discussed in section 3), in association with proliferative cells that progressively increase the cell population [13]. In our final research models, we initialise a population of cells

in a circular monolayer formation interacting via a Lennard-Jones potential. The system is left to evolve for low activity until the structure becomes more representative of a physical environment, and then the activity is stepped up, which represents a response to an environmental change. Following this shift, we seek to observe a set of regularly sized tissue fingers extending from the circular monolayer with a distinct angular frequency.

In section 2, we introduce the biological concepts and general computational models relevant to tissue organization and cell behaviour. Then, section 3 outlines the specific computational models employed in our research, which progressively increase in complexity from independent, stochastic motion, to soft particle repulsion, to a Lennard-Jones interaction. This thesis concludes with a section detailing our results, followed by a summary of what we have discovered and a consideration of future directions this branch of research may take.

2 Self-Organization in Motile Cell Systems

In this section, we first describe how intercellular connections and cell clusters form, and how this enables tissue organization. From this fundamental basis, we then outline the general mechanisms that drive tissue fingering, as well as some examples of models that have been designed to simulate this process.

2.1 Cell Clustering Behaviour

Cell clustering simply describes the formation of aggregates of cells that are both physically and functionally interconnected. Organized cell packing and cell-cell connections are essential for maintaining mechanical tissue strength, maximising the efficiency of nutrient exchange, and facilitating intercellular signalling [14]. Complex tissue architecture and organization may then arise from groups of cells capable of communication, where the resultant structure is designed for optimal execution of the specific tissue function [15]. Crucially, intercellular connections also enable the propagation of information instructing collective cell behaviour, such as co-ordinated migration towards a wound [16]. Epithelial tissue is a quintessential example of

organized, closely packed cells that exhibit collective migration [17]. In addition, epithelial monolayers are found throughout the body, such as in blood vessel and respiratory tract lining, and therefore offer comparable physical systems for our simulated cell monolayers.

Intercellular connections are mediated by cell adhesion molecules (CAMs), such as cadherins, integrins, and selectins, on cell surfaces that bind to complementary molecules on the surface of neighbouring cells [18]. The cadherin family of CAMs, in particular, is of great importance to biological cell clustering, as these transmembrane proteins are essential for the formation of adherens junctions between neighbouring cells. Adherens junctions are protein complexes that appear at cell-cell junctions in epithelial and endothelial tissue, that function to link the actin cytoskeleton between adjacent cells [19]. As the cytoskeleton mediates cell movement, these junctions are crucial for collective cell migration.

Groups of biological cells are commonly represented by agent-based or continuum-based mathematical models. Agent-based models simulate individual cells as autonomous, discrete entities that interact with each other and their environment [20]. This allows for direct integration of single-cell diversity, periodic cell injections, and cell-level processes such as cell division. In addition, agent-based models capture the differences in individual cell behaviour that are often utilised in biological processes to achieve novel functions [21]. This is seen in our research, where we identify the degree of stochastic cell behaviour that leads to the development of periodic tissue fingering. Therefore, it is appropriate for us to use an agent-based model to represent our population of cells.

On the other hand, continuum models treat clusters of cells as a continuous medium that neglects cell boundaries, and regions of cells are instead described by continuous variables. The velocity and pressure of each region of tissue then evolves according to a set of partial differential equations (PDEs) [12]. These PDEs include parameters that reference tissue properties such as viscosity, density, and growth rate, that define the response to external stresses, and the rate of change of tissue morphology. Unlike our agent-based model, continuum models are not directly applicable to our research as they are limited in their ability to capture the stochastic behaviour of individual cells.

2.2 Biological Tissue Fingering

Collectively migrating epithelial cells often display strong multicellular fingering at the leading edge of spreading tissues [2, 22]. This fingering shows similarities to viscous fingers observed in Saffman-Taylor instabilities, which occur when one viscous fluid displaces another, more viscous fluid [23]. However, epithelial monolayers are more viscous than their surroundings, and so alternative models must be constructed to represent their migration behaviour. Tissue migration fingers have been observed in physical systems from a variety of different cell types. For example, they appear during wound healing from populations of IAR-2 rat liver epithelial cells [24], as well as from MDCK (Madin-Darby canine kidney) epithelial tissue [3]. They have also been shown to develop during artificially stimulated spreading of HUVEC (human umbilical vein endothelial cells) monolayers [25], where tissue growth was induced by the addition of FGF (fibroblast growth factor). These observed examples, among others, enable in depth studies of tissue finger evolution in physical systems that are of great importance for developing accurate computational models. The occurrence of periodic tissue fingers with clear curvature and constant amplitude, rather than disordered protrusions, is significant as it suggests the presence of a coordinated, collective behavioural mechanism between the cells. Irregular fingering is indistinguishable from randomly extended cell clusters; therefore, the absence of a distinct fingering pattern in our research is considered a null result.

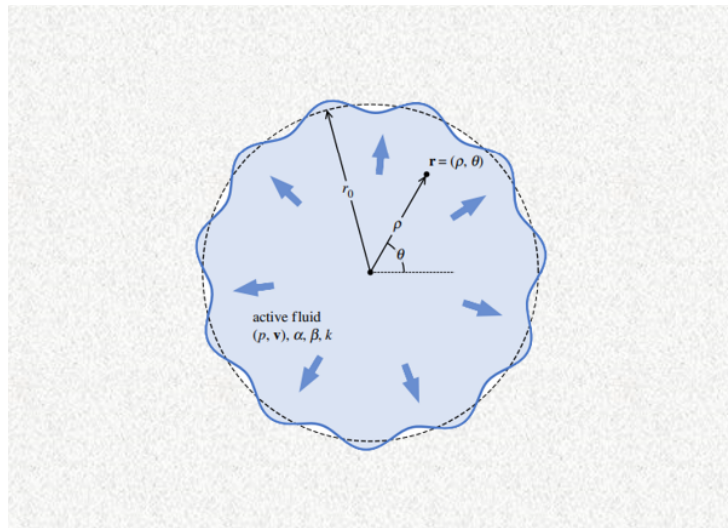


Figure 2: Active fluid model, described by Eq. 1 and Eq. 2, of a tumour expanding into external tissue exhibiting periodic tissue fingering at the interface. Modified from [12].

The appearance of tissue fingering is suggested to be led by ‘leader cells’, that initiate the formation of protrusions, with the tissue growth supported by cell proliferation [26]. Leader cells possess phenotypical properties distinct from the rest of the cell population, such as the presence of large active lamellipodium at their edges and an increased number of focal adhesions, and they are also observed to be very spread out [27]. Leader cells respond to mechanical and chemical stimuli and, in response, generate traction forces that drive directed motion into the surrounding medium. As a result, the neighbouring cells are pulled along by the ‘leaders’, forming finger-like protrusions as they migrate.

To generate tissue fingers, certain models incorporate representations of leader cells that exhibit distinct behaviour. Tarle *et al.* (2015) gave a special treatment to cells at the edge of a monolayer by implementing a curvature-motility positive feedback mechanism [28]. This is an example of a particle-based model in which cells in convex regions, such as finger-like protrusions, are assigned a motile force that increases linearly with the curvature and pulls cells outwards. On the other hand, Alert *et al.* (2019) employed an active polar fluid continuum model for epithelial spreading that does not consider any form of leader cells [22], and which includes hydrodynamic interactions throughout the tissue. Crucially, a long-wavelength instability of the leading edge was found that is simply induced by generic active traction forces at the edge of the monolayer. Our research model also seeks to find periodic fingering without implementing leader cells, though we use an agent-based model in order to control and study the behaviour of each cell throughout the tissue. Bogdan & Savin (2018) again use an active fluid model to describe fingering instabilities in tissue invasion [12]. This model was designed to represent metastatic tumour behaviour, though, like our model, is applicable to wound healing and developmental patterning, among other processes. To mathematically describe tissue evolution, pressure $p(\mathbf{r}, t)$ and velocity $\mathbf{v}(\mathbf{r}, t)$ fields follow:

$$\nabla p = -\beta \mathbf{v} + \alpha \frac{\mathbf{v}}{|\mathbf{v}|} \quad (1)$$

and

$$\nabla \cdot \mathbf{v} = k, \quad (2)$$

respectively. Here, α describes the magnitude of the active traction, and β describes the magnitude of the effective passive friction, which is proportional to the tissue viscosity. The growth rate of the tissue (as a result of cell division), is given by k . Fig. 2 displays this model tumour growing in an external tissue, which clearly differs from our agent-based model of interacting discrete entities.

3 Research Models for Motile Cell Behaviour

In this section, we outline the computational models used to describe random motion and intercellular forces in our research. When discussing each model in isolation, cells may be referred to as particles as, fundamentally, we are just applying a biological context to a particle simulation. We introduce various equations of motion and interaction potentials that progressively increase in complexity, until we are able to construct a complete system containing a population of cells with random activity and Lennard-Jones interactions from which tissue fingering may be studied.

3.1 Stochastic Motion

At the fundamental level of biological processes we see a form of ‘noise’, or stochasticity, that drives variation in the motion and behaviour of molecular components [29]. Living organisms constantly harness this stochastic variation to provide solutions to environmental challenges and generate novelty at high levels of organisation, as seen in Mendelian genetics where Brownian motion on the molecular scale leads to random fertilization [30]. Another mechanism of guided stochastic variation is observed in an immune system response to a new antigen, whereby the rate of mutations is enhanced in highly specific gene loci involved in immunoglobulin synthesis [31]. This targeted hypermutation, facilitated by the down regulation of error-correction machinery [32], enables the immune system to rapidly develop a neutralizing antibody. In the

context of this research, we add a layer of random activity to each cell's motion, on top of Lennard-Jones interactions with other cells, and investigate the effects on the development and evolution of the model tissue fingers.

We use a Brownian particle model to describe the behaviour of cells as they are subject to collisions with particles comprising the fluid suspension in which the cells are immersed. Brownian motion may be characterised as passive or active, where passive Brownian particle (PBP) motion is entirely driven by the random thermal fluctuations in the fluid, and active brownian particles (ABP) actively contribute to their own motion [33]. When we consider the effects of increasing cell activity in tissue models in this research, we do not explicitly define the specific origin of this activity. Instead, we suggest that this random activity may be sourced from a combination of both thermal fluctuations and cell self-propulsion that increases in magnitude following an environmental change, such as drug exposure or changes in an endogenous chemical gradient following tissue damage or wound formation. In this case, it is appropriate to describe the Brownian motion as having both active and passive components.

In our early model of random activity, the position \mathbf{r}_i of the i -th particle evolves according to:

$$\mathbf{r}_i(t + dt) = \mathbf{r}_i(t) + (\xi_i \sqrt{dt}) \hat{\mathbf{u}}_i, \quad (3)$$

where ξ_i is a random value, normally distributed around 0, and $\hat{\mathbf{u}}_i$ is a unit vector of random direction. Note that the magnitude of random activity is defined by the standard deviation parameter, σ , in the normal distribution for ξ . Inertia is neglected in this model as the size and speed of each particle are sufficiently small that the Reynolds number can be assumed negligible. The use of the square root of dt (or Δt to be clear that it is finite) in the equation of motion (Eq. 3) is derived from the mathematical properties of Brownian motion, whereby the displacement of particles due to random thermal fluctuations is proportional to the square root of the time interval over which it occurs. Furthermore, it is intrinsically linked to Itô calculus, which describes stochastic processes with discontinuous paths [34].

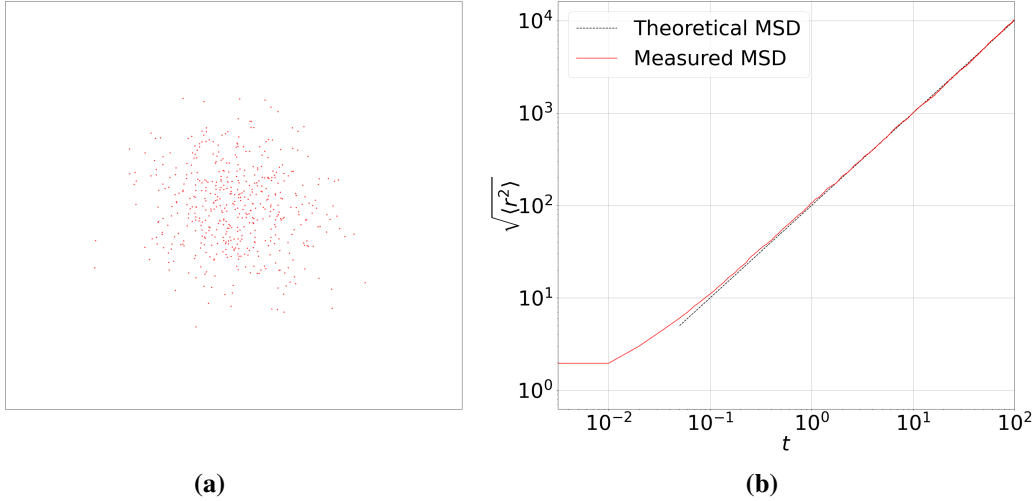


Figure 3: (a) Snapshot of $N = 1000$ Brownian particles with radius $R = 1$ at $t = 100$. Particle positions were initially set to the centre of the system, and σ was chosen to be $10R$. (b) Evolution of the measured mean squared displacement of all particles up to $t = 100$, compared with the theoretical mean squared displacement.

Crucially, for $N = 1000$ we measure a mean squared displacement (MSD) that, beyond small t , evolves with negligible differences to the theoretical model. The selected population number is on the same scale as that which is used for our simulations of tissue finger development, and so we can reliably assume that macroscopic properties of the system arising from random activity will evolve as expected in our research. The measured MSD is defined by:

$$\langle r(t)^2 \rangle = \frac{1}{N} \sum_{i=1}^N |\mathbf{r}_i(t) - \mathbf{r}_i(0)|^2, \quad (4)$$

and the theoretical MSD, calculated by taking the expected values of each element in the equation of motion (Eq. 3), is given by:

$$MSD = \sigma^2 t. \quad (5)$$

Here, we see that the variance of ξ , σ^2 , which defines the expected magnitude of random activity, is directly linked to the MSD. In a physical system, the MSD of a Brownian particle at time t follows:

$$MSD = 2dDt, \quad (6)$$

where d is the dimensionality of the system ($d = 2$ for all our models and research) and D is the diffusion coefficient [35]. The diffusion coefficient is a parameter that fundamentally describes how quickly particles will spread out due to random motion. Mathematically, it is found from the Stokes-Einstein relation [36] as:

$$D = \frac{k_B T}{6\pi R\eta}, \quad (7)$$

where k_B is the Boltzmann constant, T is the absolute temperature, R is the particle radius, and η is the viscosity of the medium. Expressing the MSD in terms of both computational and physical parameters is key to establishing a physical meaning for the random activity implemented in a computational model.

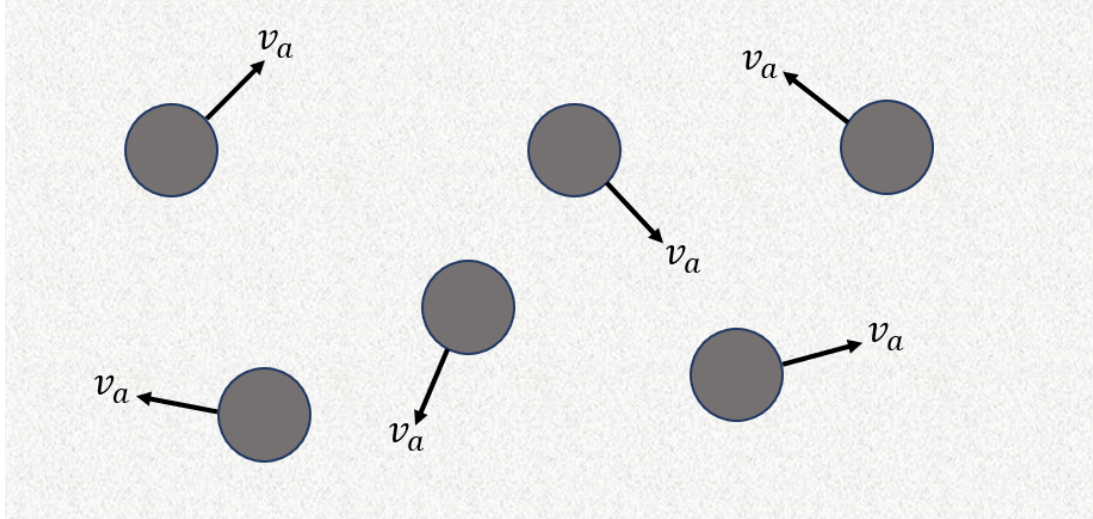


Figure 4: Example snapshot of $N = 6$ identical particles moving with an activity of magnitude v_a , and a direction defined by a uniformly random angle between 0 and 2π .

3.2 Pairwise Soft Harmonic Repulsion

Our first particle interaction model describes pairwise soft harmonic repulsion, whereby particles exert a repulsive force on their neighbours upon overlap. The interaction potential, replicated from Chacko *et al.* [10], is given by:

$$V_{ij}(r) = GR^3(1 - r/D_{ij})^2\Theta(D_{ij} - r), \quad (8)$$

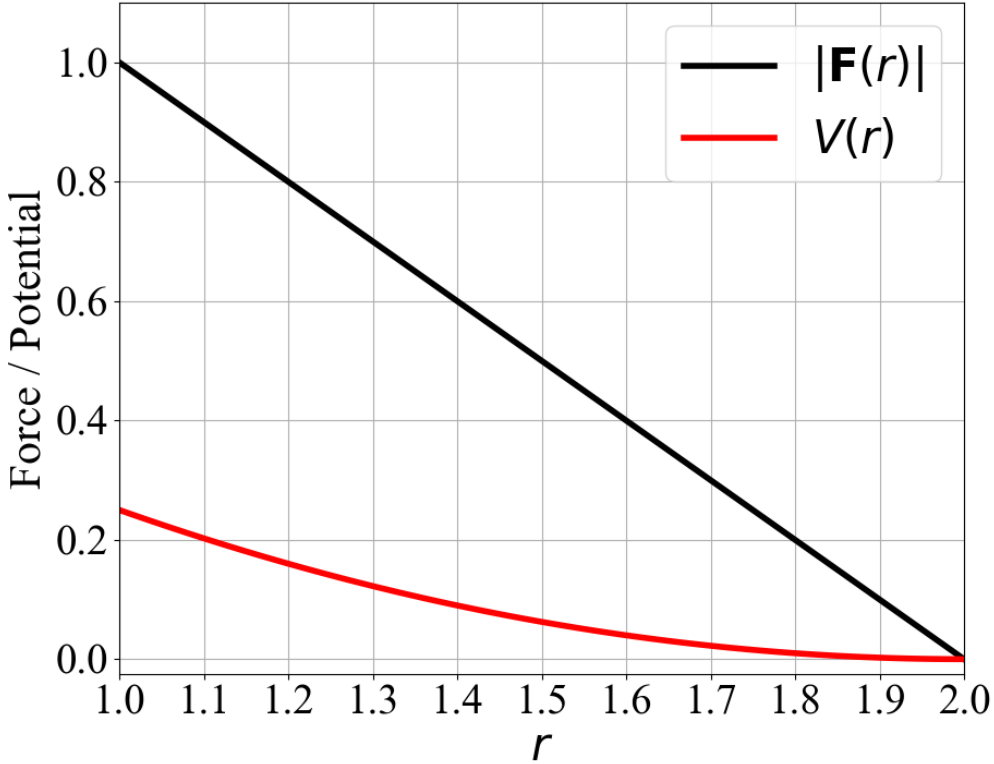


Figure 5: Variation of the magnitude of force and potential as a function of r for a soft repulsive interaction. Both R_i and $R_j = 1$.

where r is the distance between two particles, G is the particle modulus, R is the particle radius, for which we have an equal number of particles with radii R and $1.4R$, and $D_{ij} = R_i + R_j$. The argument of $\Theta(x)$ (the Heaviside function) in Eq. 8 mathematically represents the fact that the potential is equal to 0 beyond the sum of two particle radii. As a result the system tends to an equilibrium state in which no particles overlap.

We apply the interaction potential to an athermal soft particle suspension, meaning that we consider particles, capable of overlapping, that are immersed in a solvent. It is classified as athermal because particle interactions do not generate any thermal energy, and the system is not subject to any further internal or external thermal fluctuations [10]. As we are modelling behaviour in a solvent, the equation of motion requires a drag coefficient:

$$\frac{d\mathbf{r}_i}{dt} = -\frac{1}{\zeta} \sum_{j \neq i} \frac{\partial V(|\mathbf{r}_i - \mathbf{r}_j|)}{\partial \mathbf{r}_i}. \quad (9)$$

The drag coefficient, ζ , particle modulus, G , and base particle radius, R (as opposed to $1.4R$), collectively define a physical scale for the system. The drag coefficient represents the damping force on a particle's motion due to its interaction with the surrounding medium. As a result, particle velocity decreases over time, eventually reaching a stationary state. The time scale for this decay depends on the value of the drag coefficient, and this time scale can be used to describe other events in the system. The particle modulus, which characterizes particle stiffness, sets the force and stress scale as it is a measure of the relationship between an applied force and a particle's deformation [37]. The length scale of the system is simply defined by the base particle radius, which enables direct observational length assessments. For our models we set each scaling variable to 1; this is common practice as it provides a simple reference value for researchers, and allows variables to be studied in terms of relative, rather than absolute, change.

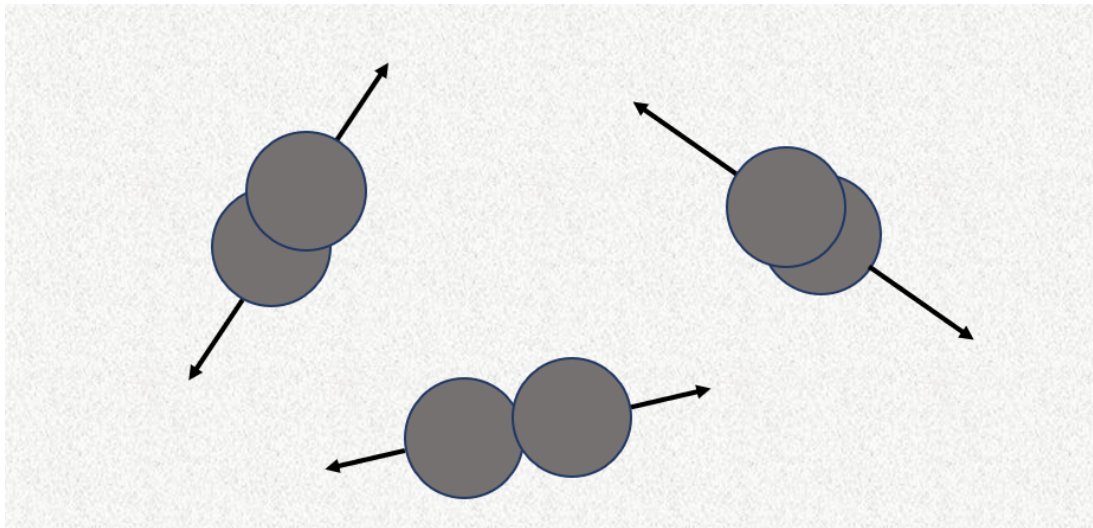


Figure 6: Example snapshot of 3 pairs ($N = 6$) of identical particles with varying degrees of overlap. Pairs of particles that are closer together repel with greater magnitude (arrows not to scale).

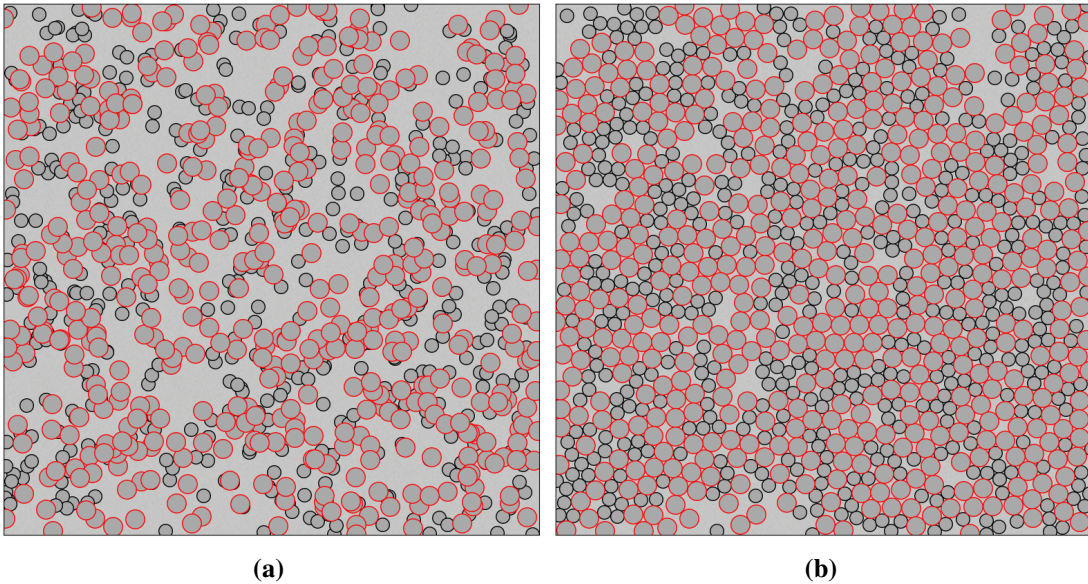


Figure 7: Evolution of an example system containing $N = 1000$ particles subject to a pairwise soft harmonic repulsion interaction potential (Eq. 8). Black and red particles have a radius of R and $1.4R$, respectively, and the system has a packing fraction of $\phi = 0.75$. (a) Initial particle positions ($t = 0$) were generated from a uniform random distribution. (b) Snapshot of the system at $t = 100$.

Fig. 7 evidences the idea that a set of particles interacting via the given potential will tend to a non-overlapping equilibrium state. The time taken to reach such a state, which is a consequence of the dissipation of kinetic energy in the system, is dependent on the fraction of the system occupied by particle area. We define a packing, or area, fraction in order to describe this property:

$$\phi = \frac{N\pi R^2}{L^2}, \quad (10)$$

where L defines the dimensions of the system. At low ϕ , particles in a system behave more like a fluid, but when ϕ exceeds ϕ_G the particles adopt a ‘glassy’ state, described as a disordered, amorphous solid exhibiting rigidity. Above $\phi_J > \phi_G$, the particles undergo a jamming transition, and they are unable to freely pass each other without rearranging the entire system [38]. As a result, the system is held in a metastable state in which relaxation times are extended and dynamics are slowed. For a system that does not consider particle elimination (apoptosis in a cellular context) or particle division, $\phi_J = 0.84$ when $d = 2$ [10]. It is then clear that the selection of ϕ during research can greatly affect system dynamics, and so it must be chosen such that the

cells maintain a somewhat fluid-like state in order to best represent a physical system.

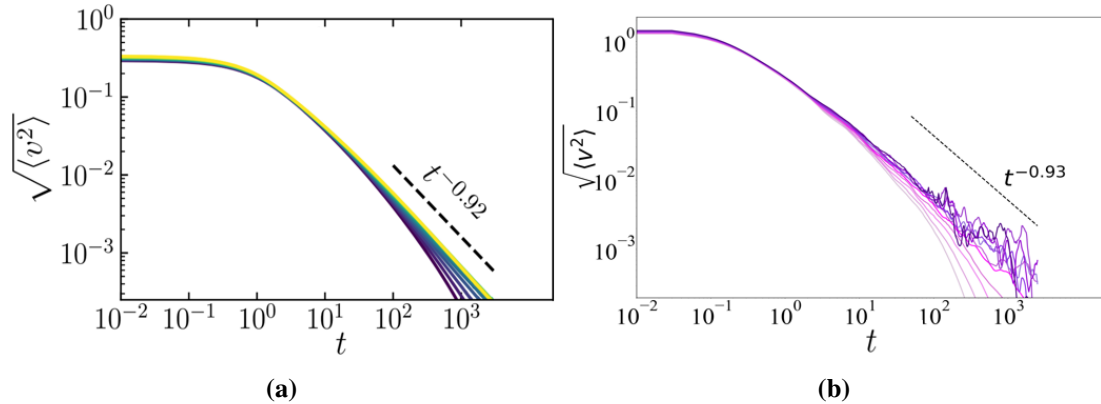


Figure 8: Decay of the root mean squared particle speed for various packing fractions over a period of $t = 0$ to 2500. $N = 10^6$ and 10^3 in (a) and (b), respectively. $\phi = 0.78, 0.8\dots 0.98, 1.00$ (curves upwards) and $d = 2$ in both systems. Subfigure (b) is a reproduction of (a), created by Chacko *et al.* [10].

The root mean squared particle speed of the system is defined as:

$$\sqrt{\langle v^2 \rangle} = \sqrt{\frac{1}{N} \sum_{i=1}^N \mathbf{v}_i \cdot \mathbf{v}_i}. \quad (11)$$

Fig. 8 shows that the decay of root mean squared particle speed enters a power law regime for this model's interaction potential. Before the packing fraction exceeds ϕ_J , the power law eventually tends to an exponential decay. However, for $\phi > \phi_J$, the power law $t^{-\beta}$ extends indefinitely as seen in Fig. 8a. For finite N , above jamming, we observe noise as the root mean squared speed approaches low values. Fig. 8 supports the claim presented by Chacko *et al.* [10] that the time at which noise appears is proportional to N . For lower N , instability in the behaviour of individual particles has a greater influence on total system dynamics. However, for $N = 1000$ we still obtain a value of $\beta = 0.93$ (calculated from a straight line fit on the logarithm of the data), a negligible difference to the compared literature value of 0.92, which further supports the validity of simulations with N chosen to be on this scale.

3.3 Lennard-Jones Interactions

In order to more accurately represent cellular activity, we build on the soft repulsion model seen in Section 3.2 by adding a long-range attraction force between particles. One common

example of a pairwise force characterized by short-range repulsion and long-range attraction is the Lennard-Jones interaction. Many forms of Lennard-Jones potentials have been used to model intermolecular and intercellular interactions [6, 39], and in our research we implement the following, common variation:

$$V_{LJ}(r) = 4\epsilon_{LJ} \left[\left(\frac{\sigma_{LJ}}{r} \right)^{12} - \left(\frac{\sigma_{LJ}}{r} \right)^6 \right]. \quad (12)$$

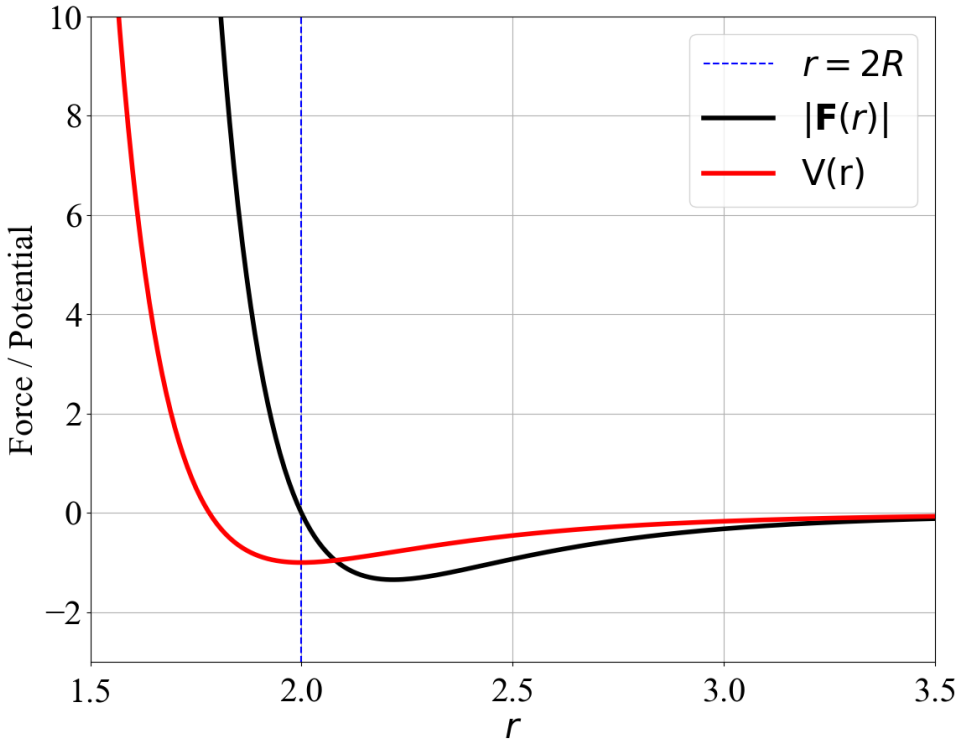


Figure 9: Variation of the magnitude of force and potential as a function of r for a Lennard-Jones interaction. Both R_i and $R_j = 1$.

We set the ‘Lennard-Jones length’ parameter $\sigma_{LJ} = D_{ij}/2^{\frac{1}{6}}$ such that the minimum of V_{LJ} is located at $r = R_i + R_j = D_{ij}$. As a result, the pairwise interaction force is 0, neither attractive or repulsive, when neighbouring particles are in contact without overlapping. The dispersion energy, ϵ_{LJ} , is set to 1, which defines the depth of the potential well ($V_{LJ,\min} = -\epsilon_{LJ}$). As this model also considers particles immersed in a fluid, designed to represent the extracellular matrix (ECM) or a culture medium in our research, the equation of motion again follows Eq. 9, with $V = V_{LJ}$ and $\zeta = 1$.

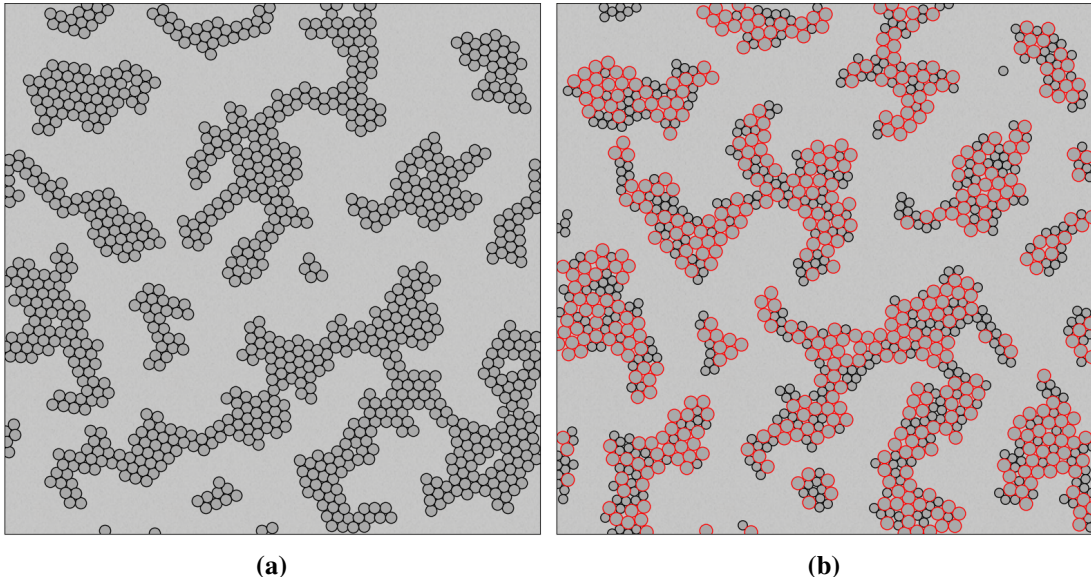


Figure 10: Snapshots of two example systems at $t = 500$ containing $N = 1000$ particles subject to a Lennard-Jones interaction potential (Eq. 12). The initial particle positions in each system were uniformly randomly generated from the same seed. (a) Monodisperse system with particle radii set to R . (b) Bidisperse system containing a mixture of particles with radii R and $1.4R$ in equal number.

Fig. 10 displays the expected clustering behaviour of particles subject to a Lennard-Jones interaction potential, which closely represents the behaviour of cells under natural environmental conditions as a result of intercellular communication and cell-cell adhesion [40]. We introduce bidispersity (Fig. 10b) to some of our research simulations in order to mimic cell diversity in physical systems, and also create another potential basis from which periodic tissue fingering may develop. In addition, particle-size polydispersity hinders crystallization of isotropic particles [41]. This is key to limiting the occurrence of artifacts in our results, as well as ensuring that the particles do not form an overly static structure from which realistic dynamics and tissue migration cannot occur. Adding a layer of random activity, described in Section 3.1, to the Lennard-Jones model inevitably promotes the disruption of cluster formations, and so combining these models enables research into the dynamics of cell cluster breakaway and tissue fingering.

As our models grow in complexity, and computational cost increases, we must implement a set of compensating features. As the repulsive force component of the Lennard-Jones interaction extends asymptotically to infinity as r approaches 0, we require an adaptive timestep. The adaptive timestep is scaled by the inverse maximum particle speed, $\Delta t(t) = a/v_{max}(t)$, where

the selection of a defines the maximum distance any particle may travel in a given timestep. The computational cost of particle simulations with large N is so high due to the $\mathcal{O}(N^2)$ relationship for particle-particle distance and pairwise force calculations. However, at large r , the magnitude of the force is effectively 0, so we include a Verlet neighbour list to only consider interactions between particles that are mutually located within their cutoff radii [42]. This significantly increases efficiency, and particle positions deviate negligibly from simulations considering all N^2 interactions. Finally, we enact periodic boundary conditions and incorporate a nearest neighbour search. Periodic boundary conditions simulate an infinite system by imposing periodicity in both spatial dimensions, whereby any particle that goes beyond the defined system dimensions reappears at the opposite limit. This ensures that particle number and density remains constant, without artificially imposing a boundary with a repulsive potential at the ‘walls’ of the system that would otherwise affect particle dynamics. To further strengthen the idea of an infinite system, we reproduce our box of particles 8 times to form a 3x3 grid. When calculating the distance, r , between the i-th and j-th particle, we use a nearest neighbour search, so r is defined as the smallest of all distances between the i-th particle in the central box, and the 9 identical j-th particles in the 3x3 grid.

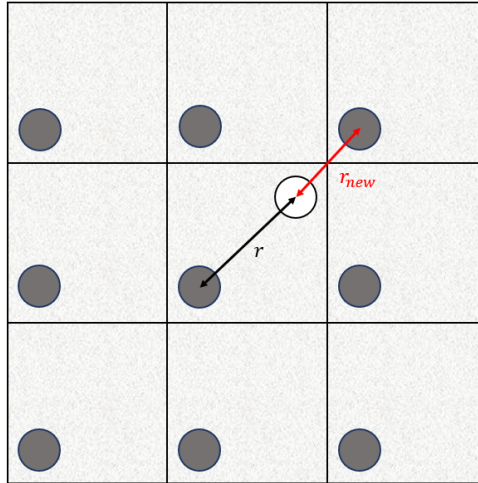


Figure 11: Example of an update to the variable r from a nearest neighbour search in a system with $N = 2$. White and grey particles represent the i-th and j-th particles, respectively. For simplicity, only the position of the j-th particle is reproduced in each grid element.

4 Results & Discussion

In our study of the emergence of periodic tissue fingering, cells display some random motion and interact via a Lennard-Jones potential, described in section 3.3. From Eq. 3, we update our model of stochastic behaviour to fix the magnitude of random activity, whilst keeping the direction of motion to be random.

$$\mathbf{r}_i(t + dt) = \mathbf{r}_i(t) + (v_a \sqrt{dt}) \hat{\mathbf{u}}_i. \quad (13)$$

The parameter v_a is referred to as 'active swim speed', or simply 'activity', and is manually varied between different simulations as we search for the critical activity range at which periodic tissue fingering occurs.

4.1 Cell Activity Affects Cluster Stability

A population of cells interacting via a Lennard-Jones potential will form a stable cluster. When a layer of activity is added to this model, we expect that the cluster remains stable and orderly for low v_a , which we study in Regime 1 of our research, and breaks apart violently for high v_a , seen in Regime 2. The expected result of Regime 1 is shown in Fig. 10, with $v_a = 0$.

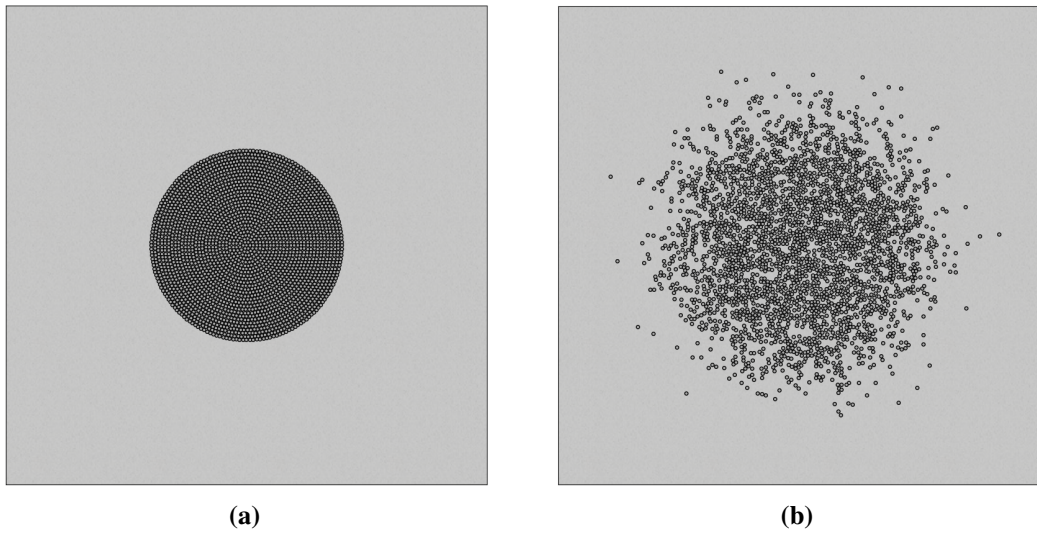


Figure 12: Regime 2: $N = 2553$ cells interacting via a Lennard-Jones potential, with $v_a = 1.8$ and $\zeta = 1$. (a) Snapshot of the initial setup of the system ($t = 0$). (b) Snapshot of the system at $t = 180$.

At a critical v_a , or critical range of v_a , between these activity extremes, the tissue structure must become dynamic while still maintaining cell-cell adhesion. Therefore, in Regime 3, we seek to find this range of activity as it provides the conditions for periodic tissue fingering to occur.

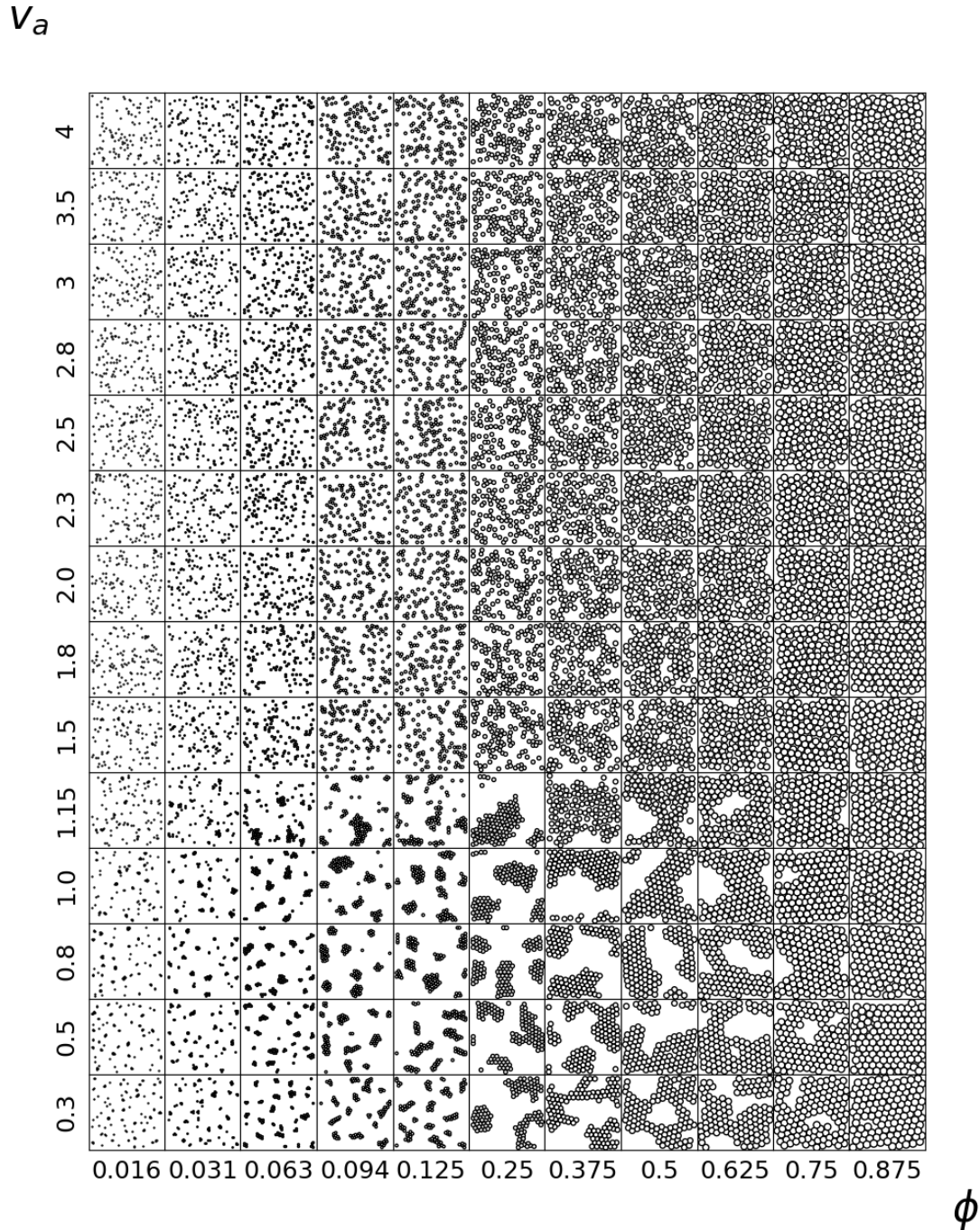


Figure 13: $N = 121$ cells interacting via Lennard-Jones with varying activity. $\zeta = 1$. Snapshots of the state of each system for various packing fractions are shown at $t = 5 \times 10^2/v_a$. Each system was initialised at $t = 0$ in a random state. Reproduced from Navarro & Fielding (2015) [6].

In Fig. 13, we see that the activity for which the system transitions from a clustered formation

to a disordered state lies between $v_a = 1.15$ and $v_a = 1.5$ over the selected time period. This observational deduction is particularly evident for $\phi = 0.25$. Notably, at high packing fractions and low activity, we see solid-like ordering. However, at $v_a = 1.5$ and above, there is clear cell overlap and ordering instability which suggests that, above this activity, the pairwise attraction forces are overwhelmed and cells break away from their neighbours, which is an undesired effect for fingering development. This sets an upper limit of activity for which fingering may occur. We cannot explicitly define a lower limit at this stage as, after extreme lengths of time, fingering could possibly occur in any system where cell-cell adhesion is maintained for a particular low activity. Therefore, our lower limit is instead determined by the maximum realistic length of time that our simulations may be run for.

4.2 Periodic Protrusions Occur at a Critical Activity

In Regime 3 we trial a large set of values of v_a and isolate a range of activity for which finger-like protrusions may develop in a monodisperse system for our time frame (up to $\sim t = 600$). For $N = 1000$, this range is $\sim 1.05 < v_a < 1.16$, and for $N = 2500$, this range is $\sim 1.08 < v_a < 1.20$. Note that these limits are observationally determined, and the lower limit is dependent on the maximum time achieved. At a critical activity of $v_a = 1.1$, for $N = 963$, we generated periodic protrusions from a model tissue. However, we are unable to reproduce this result for another random seed, or for any other combination of N and v_a . Also, as fingers regular developed and faded away throughout the evolution of the example system, it is possible that the appearance of periodic protrusions is a temporary, chance-based event in which each protrusion appeared in a favourable organization. Therefore, this result is inconclusive, and we cannot confidently define these protrusions as periodic tissue fingers given the implication of a reproducible collective behavioural mechanism driving the process.

In order to quantitatively define and measure the periodicity of finger-like protrusions in these systems, we must first define a perimeter around the cluster of cells. To do this, we start by dividing the system into a fine grid of unit dimensions. Each grid square, shown in Fig. 14b, is assigned a value of 1 if it is within a radius, r_a , of a cell, and 0 otherwise. r_a , chosen to be

$3R$, defines a cell's 'influence area'. We implement an influence area from each cell so as to avoid marking 'internal voids', or simply gaps, within the body of cells. Furthermore, 'splinter' cells that are located far from any other cell do not influence grid scoring. Using this scoring system, we then record the coordinates of the centre of each grid square that has a score of 0, and that also exists next to a grid square with a score of 1. These boundary coordinates are then used to plot the perimeter of the shape. From the centre of the system to our defined perimeter, we run a sweep from $\theta = 0$ to 2π , and record the radius, r , of the shape at regular small angle intervals (Fig. 15). This data allows us to compute a fast Fourier transform (FFT), which provides information on the angular frequencies of tissue finger occurrence. Any distinct peak seen in the FFT analytically confirms periodic tissue fingering, and is a direct measurement of the associated angular frequency.

The cells were initialised in a circular monolayer structure with $v_a = 0.3$. The activity is then 'turned on', whereby v_a is increased to the value being investigated, after the system is given sufficient time to generate a more realistic and random tissue organization (experimentally determined to be $\sim t = 5$).

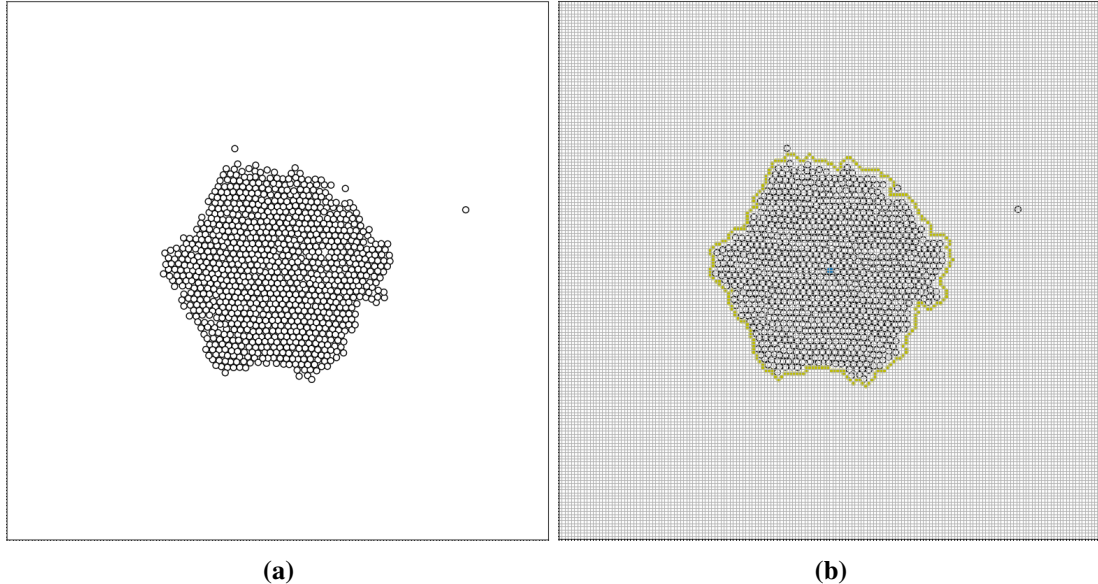


Figure 14: $N = 963$, $v_a = 1.1$. (a) Snapshot of the state of the system at $t = 500$. (b) Computationally-drawn perimeter defining the shape of the tissue.

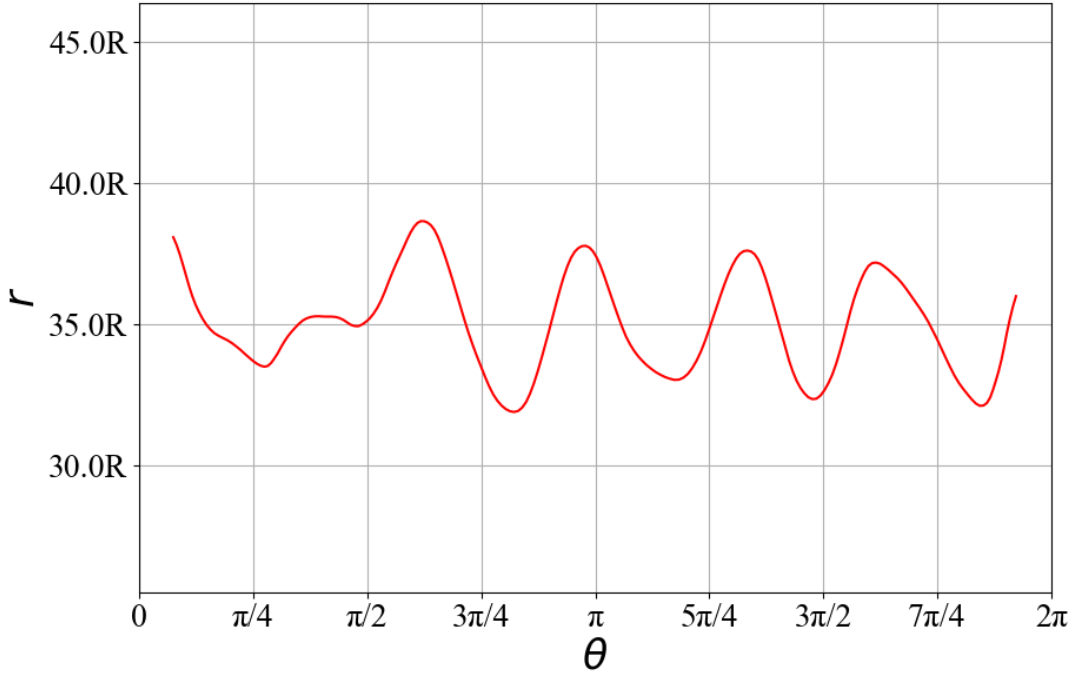


Figure 15: Variation of cell cluster radius, r (measured to perimeter seen in Fig. 14b), against the angle, θ , from the centre of the system. Data ‘smoothed’ using an exponential moving average (EMA).

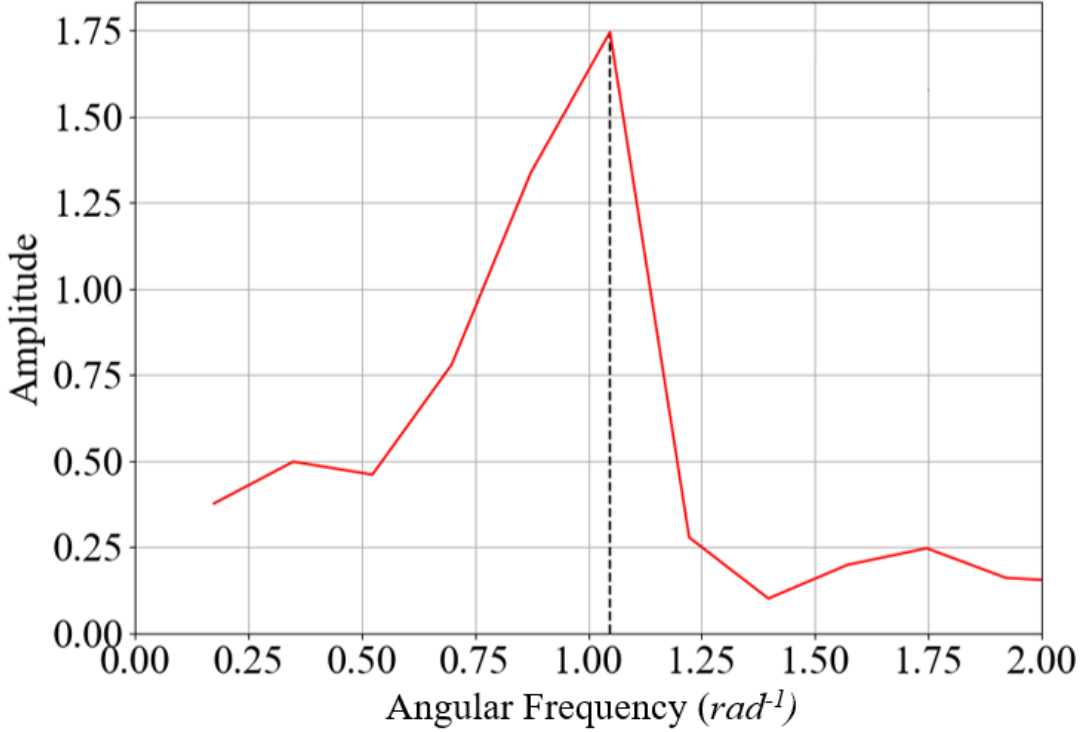


Figure 16: FFT of the data presented in Fig. 15, peak corresponds to an angular frequency of 1.05rad^{-1} .

We see a (perturbed) sinusoid in Fig. 15 which represents the periodic protrusions seen in an angular sweep of this cell cluster. This is the desired form of this measured function when seeking periodic tissue fingering. However, as mentioned, the causation of this result is

inconclusive. Note that an EMA is applied to smooth uncertainty in the measurement of the perimeter. Such uncertainty arises as our grid squares have finite dimensions, so the curve does not consider each infinitesimal point around the shape. Furthermore, inaccuracy is generated as a consequence of the influence area, as finger amplitudes become a smaller proportion of the base circular monolayer radius as r_a increases from 0. At high r_a , deviations in r corresponding to finger occurrence would be indistinguishable from noise. However, greater inaccuracy would arise if this system were not incorporated, as internal voids would perturb the boundary measurement.

In summary, for $v_a = 1.1$ and $N = 963$, we observe periodic protrusions with an angular frequency of 1.05rad^{-1} , which corresponds to the occurrence of a protrusion every 0.305π . This peak is found despite the lack of definition in 1 of 6 expected protrusions (based on the angular frequency) in Fig. 14. Although these results suggest the possibility of periodic tissue fingering arising from fundamental behaviour, they are inconclusive due to a lack of reproducibility and the possibility of alternate causation (crystallization or chance). It is possible that periodic tissue fingering from this model is reproducible for larger N , studied over longer time periods, however, we were unable to research all possibilities due to computational constraints.

4.3 Bidispersity

A bidisperse system is implemented to more accurately mimic cell diversity observed in physical systems, in addition to preventing crystallization of the cell population. For $v_a = 1.145$ and $N = 2553$ (Fig. 17), we see regularly repeating small-amplitude fingers protruding from the right-hand side of the tissue. However, this periodicity does not appear for a full sweep of 0 to 2π with any set of parameters. For $N = 2553$, we observe similarly localised periodicity throughout the range of $1.08 < v_a < 1.2$, and, crucially, there are no signs of crystallization and the fingers exhibit a true curvature, unlike our monodisperse system. Although we fail to find complete periodic fingering in this model, the results are promising. Further research, facilitated by increased computational power, may well yield reproducible, complete tissue fingering for a particular range of v_a over a longer time period.

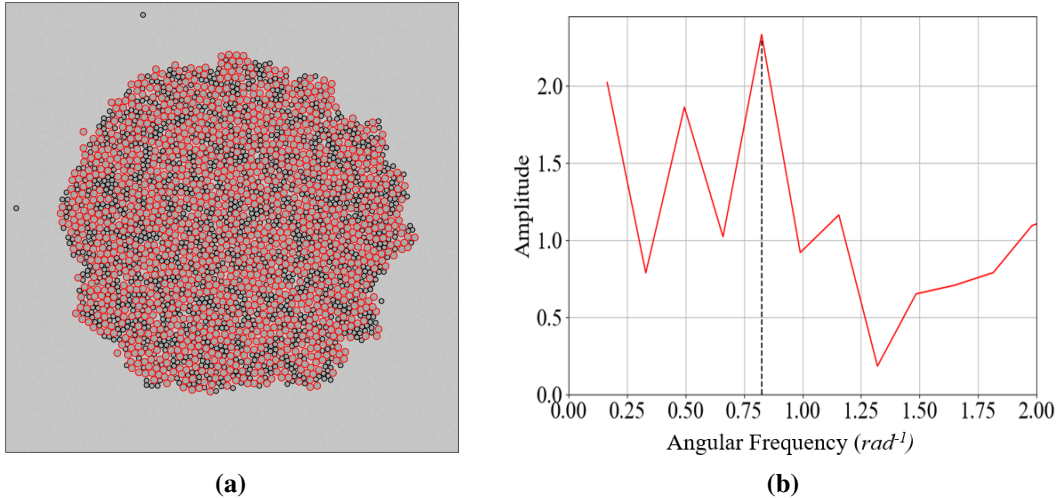


Figure 17: (a) Snapshot of a bidisperse system at $t = 500$. $N = 2553$, $v_a = 1.145$, $R_1 = R$ (black), $R_2 = 1.4R$ (red). (b) FFT of data measuring r against θ , peak corresponds to $0.825 rad^{-1}$.

4.4 Tissue Growth

In this model, we simulate tissue growth, that arises from cell division in physical systems, by implementing periodic cell injections, which refers to the addition of new cells at regular intervals (Δt_{inj}). We hypothesize that incorporating tissue growth to our monodisperse system will facilitate the development of periodic tissue fingering from the collective behaviour of motile cells.

For $v_a = 1.085$ and initial $N = 2553$ (Fig. 18), we observe a distinct angular frequency at which extensions from the centre of the tissue appear. This angular frequency is found to be $1.01 rad^{-1}$, which corresponds to a protrusion every 0.315π . Visually, we can see 6 clear vertices on the perimeter of the tissue which lead to measurements of r against θ that are very similar to that of perfect periodic tissue fingers. However, as was found for the results of our first monodisperse system, outlined in Section 4.2, the periodic extensions exhibit little to no curvature and are characteristic of a highly crystallized structure. Notably, this general structure is observed throughout the range of $1.08 < v_a < 1.2$ for an initial N of 2553. Ultimately, we assume that this measured periodicity is merely a result of crystallization in a monodisperse system, which renders this a null result.

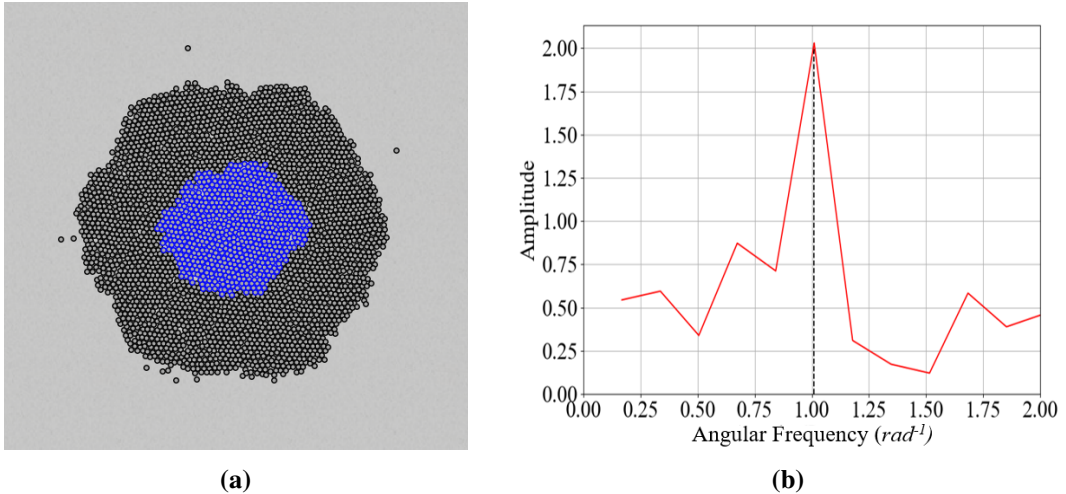


Figure 18: (a) Snapshot of a system at $t = 400$. $\Delta t_{inj} = 0.6$, $v_a = 1.085$. Number of cells grows from $N = 2553$ to 3254 between $t = 0$ and 400 . Injected cells are marked as blue. (b) FFT of data measuring r against θ , peak corresponds to 1.01rad^{-1} .

5 Conclusion & Future Perspectives

Inspired by the development of finger-like protrusions from spreading epithelial tissue in physical systems and alternative research models, we constructed an agent-based active matter model to study the fundamental origin of periodic tissue fingering. By modelling the population of cells as a circular monolayer interacting via a Lennard-Jones potential, and neglecting leader cells, we generate results showing that the origin of this phenomenon may be simply derived from the collective behaviour of motile cells exhibiting stochastic behaviour. However, this is not conclusive. In addition, it is clear that there is a narrow range of critical activity (dependent on N, ζ) for which the conditions for tissue finger development are present, whereby cell adhesion is maintained, but the cells are active enough to drive dynamic collective behaviour.

In a monodisperse system, periodic protrusions appear with and without tissue growth. However, we attribute this to crystallization of the system, rather than the collective behaviour of motile cells with stochastic motion. Therefore, we suggest that the localised periodicity observed in our bidisperse system is a more valid result with respect to our research objective, and offers more potential as an avenue of further research aiming to analyse the development of

periodic fingering as a pure result of collective cell motility.

When unbound by computational limitations, running simulations for higher N , over longer periods of time, may possibly yield a set of parameters that generate reproducible periodic tissue fingers. In addition, tissue growth in a bidisperse system (for various Δt_{inj}), or a variation of initial conditions, may also provide the conditions necessary to achieve the research objective. If one were to find conditions where periodic fingering is reproducible without crystallization, it would be interesting to see the results of measurements of the variation of finger amplitude, as well as the angular frequency, against increasing N and v_a .

Future research could benefit from establishing a more direct link between computational models and physical systems, such as wound healing, embryonic development, or tumour invasion environments. To do this, the system could be studied in 3 dimensions, and parameters could be selected to represent real properties, such as the drag coefficient, polydisperse cell radii and, crucially, the value of v_a when the system is in a natural state, as well as a perturbed state in which fingering has been seen to occur.

References

- [1] Ricard V Solé, Daniel López, Marta Ginovart, and Joaquim Valls. Self-organized criticality in monte carlo simulated ecosystems. *Physics Letters A*, 172(1-2):56–61, 1992.
- [2] Tobias Büscher, Angel L Diez, Gerhard Gompper, and Jens Elgeti. Instability and fingering of interfaces in growing tissue. *New journal of physics*, 22(8):083005, 2020.
- [3] Mathieu Poujade, Erwan Grasland-Mongrain, A Hertzog, J Jouanneau, Philippe Chavrier, Benoît Ladoux, Axel Buguin, and Pascal Silberzan. Collective migration of an epithelial monolayer in response to a model wound. *Proceedings of the National Academy of Sciences*, 104(41):15988–15993, 2007.
- [4] David Gonzalez-Rodriguez, Karine Guevorkian, Stéphane Douezan, and Françoise Brochard-Wyart. Soft matter models of developing tissues and tumors. *Science*, 338(6109):910–917, 2012.
- [5] Denise J Montell. Border-cell migration: the race is on. *Nature reviews Molecular cell biology*, 4(1):13–24, 2003.
- [6] Ricard Matas Navarro and Suzanne M Fielding. Clustering and phase behaviour of attractive active particles with hydrodynamics. *Soft Matter*, 11(38):7525–7546, 2015.
- [7] Gao Wang, Trung V Phan, Shengkai Li, Michael Wombacher, Junle Qu, Yan Peng, Guo Chen, Daniel I Goldman, Simon A Levin, Robert H Austin, et al. Emergent field-driven robot swarm states. *Physical review letters*, 126(10):108002, 2021.
- [8] Xiaoyu Chen, Paola Carbone, Giuseppe Santangelo, Andrea Di Matteo, Giuseppe Milano, and Florian Müller-Plathe. Backmapping coarse-grained polymer models under sheared nonequilibrium conditions. *Physical Chemistry Chemical Physics*, 11(12):1977–1988, 2009.

- [9] Tamás Vicsek, András Czirók, Illés J Farkas, and Dirk Helbing. Application of statistical mechanics to collective motion in biology. *Physica A: Statistical Mechanics and its Applications*, 274(1-2):182–189, 1999.
- [10] Rahul N Chacko, Peter Sollich, and Suzanne M Fielding. Slow coarsening in jammed athermal soft particle suspensions. *Physical review letters*, 123(10):108001, 2019.
- [11] Étienne Fodor and M Cristina Marchetti. The statistical physics of active matter: From self-catalytic colloids to living cells. *Physica A: Statistical Mechanics and its Applications*, 504:106–120, 2018.
- [12] Michał J Bogdan and Thierry Savin. Fingering instabilities in tissue invasion: an active fluid model. *Royal Society open science*, 5(12):181579, 2018.
- [13] Yanjun Yang and Herbert Levine. Leader-cell-driven epithelial sheet fingering. *Physical biology*, 17(4):046003, 2020.
- [14] Roberto Bruzzone, Thomas W White, and David L Paul. Connections with connexins: the molecular basis of direct intercellular signaling. *European Journal of Biochemistry*, 238(1):1–27, 1996.
- [15] Alişya A Anlaş and Celeste M Nelson. Tissue mechanics regulates form, function, and dysfunction. *Current opinion in cell biology*, 54:98–105, 2018.
- [16] Guru-Dutt Sharma, Jiucheng He, and Haydee EP Bazan. p38 and erk1/2 coordinate cellular migration and proliferation in epithelial wound healing: evidence of cross-talk activation between map kinase cascades. *Journal of Biological Chemistry*, 278(24):21989–21997, 2003.
- [17] Eric Theveneau and Roberto Mayor. Collective cell migration of epithelial and mesenchymal cells. *Cellular and Molecular Life Sciences*, 70:3481–3492, 2013.
- [18] Barry M Gumbiner. Cell adhesion: the molecular basis of tissue architecture and morphogenesis. *Cell*, 84(3):345–357, 1996.
- [19] Alpha S Yap, William M Brieher, and Barry M Gumbiner. Molecular and functional analysis of cadherin-based adherens junctions. *Annual review of cell and developmental biology*, 13(1):119–146, 1997.
- [20] Thomas E Gorochowski. Agent-based modelling in synthetic biology. *Essays in biochemistry*, 60(4):325–336, 2016.
- [21] Ertugrul M Ozbudak, Mukund Thattai, Han N Lim, Boris I Shraiman, and Alexander Van Oudenaarden. Multistability in the lactose utilization network of escherichia coli. *Nature*, 427(6976):737–740, 2004.
- [22] Ricard Alert, Carles Blanch-Mercader, and Jaume Casademunt. Active fingering instability in tissue spreading. *Physical review letters*, 122(8):088104, 2019.
- [23] Philip Geoffrey Saffman and Geoffrey Ingram Taylor. The penetration of a fluid into a porous medium or hele-shaw cell containing a more viscous liquid. *Proceedings of the Royal Society of London. Series A. Mathematical and Physical Sciences*, 245(1242):312–329, 1958.
- [24] T Omelchenko, JM Vasiliev, IM Gelfand, HH Feder, and EM Bonder. Rho-dependent formation of epithelial “leader” cells during wound healing. *Proceedings of the National Academy of Sciences*, 100(19):10788–10793, 2003.
- [25] Philip Vitorino and Tobias Meyer. Modular control of endothelial sheet migration. *Genes & development*, 22(23):3268–3281, 2008.

- [26] Amin Doostmohammadi, Sumesh P Thampi, Thuan B Saw, Chwee T Lim, Benoit Ladoux, and Julia M Yeomans. Celebrating soft matter's 10th anniversary: Cell division: a source of active stress in cellular monolayers. *Soft Matter*, 11(37):7328–7336, 2015.
- [27] Vincent Hakim and Pascal Silberzan. Collective cell migration: a physics perspective. *Reports on Progress in Physics*, 80(7):076601, 2017.
- [28] Victoria Tarle, Andrea Ravasio, Vincent Hakim, and Nir S Gov. Modeling the finger instability in an expanding cell monolayer. *Integrative Biology*, 7(10):1218–1227, 2015.
- [29] Denis Noble. The role of stochasticity in biological communication processes. *Progress in Biophysics and Molecular Biology*, 162:122–128, 2021. On the Physics of Excitable Media. Waves in Soft and Living Matter, their Transmission at the Synapse and their Cooperation in the Brain.
- [30] Erwin Frey and Klaus Kroy. Brownian motion: a paradigm of soft matter and biological physics. *Annalen der Physik*, 517(1-3):20–50, 2005.
- [31] Valerie H Odegard and David G Schatz. Targeting of somatic hypermutation. *Nature Reviews Immunology*, 6(8):573–583, 2006.
- [32] Huseyin Saribasak and Patricia J Gearhart. Does dna repair occur during somatic hypermutation? In *Seminars in immunology*, volume 24, pages 287–292. Elsevier, 2012.
- [33] Giorgio Volpe, Sylvain Gigan, and Giovanni Volpe. Simulation of the active brownian motion of a microswimmer. *American Journal of Physics*, 82(7):659–664, 2014.
- [34] V. Balakrishnan. *Brownian Motion*, pages 107–128. Springer International Publishing, Cham, 2021.
- [35] Eiji Yamamoto, Takuma Akimoto, Ayori Mitsutake, and Ralf Metzler. Universal relation between instantaneous diffusivity and radius of gyration of proteins in aqueous solution. *Physical review letters*, 126(12):128101, 2021.
- [36] MA Islam. Einstein–smoluchowski diffusion equation: a discussion. *Physica Scripta*, 70(2-3):120, 2004.
- [37] C Thornton and SJ Antony. Quasi–static deformation of particulate media. *Philosophical Transactions of the Royal Society of London. Series A: Mathematical, Physical and Engineering Sciences*, 356(1747):2763–2782, 1998.
- [38] Andrea J Liu and Sidney R Nagel. The jamming transition and the marginally jammed solid. *Annu. Rev. Condens. Matter Phys.*, 1(1):347–369, 2010.
- [39] S-P Fu, Zhangli Peng, Hongyan Yuan, R Kfouri, and Y-N Young. Lennard-jones type pair-potential method for coarse-grained lipid bilayer membrane simulations in lammps. *Computer Physics Communications*, 210:193–203, 2017.
- [40] S Jonathan Singer. Intercellular communication and cell-cell adhesio n. *Science*, 255(5052):1671–1677, 1992.
- [41] Flavio Romano, John Russo, and Hajime Tanaka. Influence of patch-size variability on the crystallization of tetrahedral patchy particles. *Physical review letters*, 113(13):138303, 2014.
- [42] Loup Verlet. Computer” experiments” on classical fluids. i. thermodynamical properties of lennard-jones molecules. *Physical review*, 159(1):98, 1967.

Acknowledgements

In particular I'd like to express gratitude towards my supervisors Prof Suzanne Fielding and Dr Michael Hertaeg for the chance to work on this project, and for continuous support throughout the duration of the academic year.